Dynamics of surface-excitonic emission in ZnO nanowires

L. Wischmeier,* T. Voss,† I. Rückmann, and J. Gutowski
Institute of Solid State Physics, University of Bremen, P.O. Box 330440, D-28334 Germany

A. C. Mofor, A. Bakin, and A. Waag
Institute of Semiconductor Technology, Technical University of Braunschweig, Hans-Sommer-Strasse 66, D-38106 Braunschweig, Germany

(Received 8 August 2006; revised manuscript received 20 September 2006; published 22 November 2006)

We report on systematic investigations of the dynamics of the surface-excitonic (SX) near-band-edge photoluminescence of ZnO nanowires observed at ≈3.365 eV. The temporal evolution of the SX emission of vapor-phase grown ZnO nanowires with diameters of d=40–130 nm is studied as a function of spectral position, temperature, and excitation intensity. A phenomenological rate-equation model is developed and discussed which is able to describe the experimentally observed transients pointing to a biexponential decay. A detailed analysis shows that the dependence of the transients on the spectral position can be explained by the relaxation and decay of excitons that are separated into a strongly localized and another weakly localized fraction. With increasing temperature, the trapped excitons are activated into less localized SX centers at higher lying energies. The distinct SX emission saturation behavior with increasing excitation density observed in time-integrated as well as in time-resolved measurements is clearly related to the limited number of SX near-surface centers.

DOI: 10.1103/PhysRevB.74.195333 PACS number(s): 78.67.Bf, 73.20.−r, 78.55.Et

I. INTRODUCTION

Nanostructures have attracted much attention in recent years since they can be reproducibly fabricated and are promising building blocks for nanometer-scale electronic and photonic devices.[1–9] New methods have been developed to fabricate a large variety of structures[5,6,9–12] whose particular features depend on the precise growth conditions, substrates, and catalysts. Especially, self-assembled nanowires and nanorods offer a large variety of interesting and unique properties since they turned out to grow in rather excellent quality even in relatively simply controllable processes and to become nearly strain-free under these conditions.

In particular, ZnO nanowires and nanorods attracted renewed attention in recent years due to their peculiar optical properties.[2,9,13,14] ZnO is a direct wide band-gap semiconductor exhibiting near band-edge photoluminescence (PL) in the UV spectral region (E_{gap}=3.37 eV at room temperature) and an exciton binding energy of 60 meV, with the latter being significantly larger compared to the thermal energy $k_BT \approx 25$ meV at RT.[1,2,14] Therefore, this material system is a promising candidate for short-wavelength optoelectronic devices. The attention on ZnO has grown considerably since the first report on a light-emitting diode based on p-doped ZnO was published.[15] Concepts for technological applications such as light-emitting diodes, laser diodes, transistors, solar cells, and sensors[1,7,15–19] have been developed in recent years. However, for any application a detailed knowledge about the optical properties and their microscopic origin, which are influenced by, e.g., growth methods or the geometry of the nanostructures, are of fundamental importance. They have to be carefully determined to either suppress undesirable features or to even make use of specific characteristics for the design and operation of future ZnO-based devices.

Even though the optical properties of ZnO nanowires with thicknesses beyond 40 nm are not yet noticeably affected by quantum effects and are thus mainly determined by the well-known properties of ZnO bulk material, the influence of the near-surface region considerably increases with decreasing wire diameter. Due to the large surface-to-volume ratio determined by the small diameter of the nanowires, these structures are an ideal system to analyze the influence of the surface on the optical properties. In Ref. 20 we analyzed the PL dependence on the diameter of individual ZnO nanowires. It was shown that especially in nanowires with decreasing diameter a rather prominent near band-edge PL peak at ≈3.367 eV increasingly contributes to the optical properties of individual wires and was thus assigned to the recombination of surface excitons (SX). This finding corresponds to the results reported by Grabowska *et al.*[21] and Travnikov *et al.*,[22,23] where a ZnO-nanowire/nanowall system and a specially treated bulk ZnO crystal were investigated, respectively. Further investigation of the origin and dynamics of this SX near-band-edge emission is of particular importance for the design of ZnO-based nanowire structures. The study of the dynamics of the SX emission reveals detailed information about its origin.

In this paper, we report on systematic investigations of the SX dynamics by use of spectrally selective and time-resolved measurements. We investigate the SX emission-band dynamics spectrally resolved as a function of temperature and excitation intensity. A simple rate-equation model is developed to discuss and interprete the obtained experimental results.

II. EXPERIMENTAL DETAILS

The ZnO nanowire/nanowall sample was grown on a 6H-SiC substrate by a vapor-phase epitaxy (VPE) technique.[24] For this technique the substrate is placed on a quartz plate in an oven. The pure metal Zn is transported directly to the

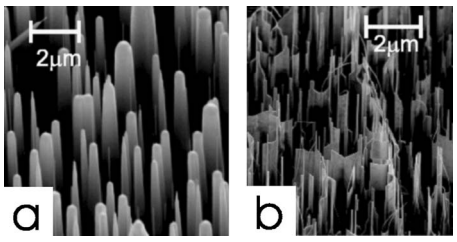

FIG. 1. Scanning-electron-microscopy (SEM) images of the ZnO nanowire/nanowall ensemble grown by the VPE method on a 6H-SiC substrate.

substrate by use of N_2 as carrier gas while O_2 is introduced via another gas line. The sample was grown at 750 °C and a pressure of 10 mbar.

Figure 1 shows two nanorod samples obtained from the VPE system. Figure 1(a) shows singly standing nanorods that can form the basis for single nanodevices possessing optical properties similar to the ones investigated in Ref. 20. Opposite to this, Fig. 1(b) shows nanowires with relatively large aspect ratio, which grew perpendicular to the substrate and are in some cases connected with thin nanowalls in the lower half of the total length. The wires have a length in the range of $l=2$ to 6 μm and a diameter of $d=40$ to 130 nm. The small diameter of the wires in comparison to their length leads to a more pronounced contribution of the surface on the optical properties in comparison to the wires with $d=90$ to 620 nm investigated in Ref. 20. Since surface excitonic emission would be clearly visible with such samples, the structures depicted in Fig. 1(b) were considered for these studies.

For the investigation of the optical properties of the ZnO nanostructures a micro-photoluminescence setup is used that is similar to the one described in Ref. 20. As light source, a frequency-doubled Ti:sapphire laser provides ≈100 fs pulses with a repetition rate of 82 MHz at 3.542 eV (corresponding to a wavelength of 350 nm) so that the sample is excited nonresonantly. The laser light is focused via a microscope objective onto the sample. The emitted PL is collected by the same microscope objective and is recorded spectrally resolved by a combination of a spectrometer and a liquid-nitrogen cooled CCD camera. The spatial resolution determined by the laser-spot diameter is about 2 μm.

For time-resolved measurements the time-correlated single-photon counting technique (TCPC) is used. This technique yields the probability distribution of the delay time between the excitation pulse and the single signal PL photons and thus represents the time evolution of the PL signal. For this technique the fundamental infrared emission of the laser pulses is detected by a fast photodiode and used as reference signal in time. The single signal photons are detected by a multi channel plate mounted behind a spectrometer. The complete system provides a spectral resolution of ≈2.4 meV and a time resolution of about 30 ps which is limited by the response time of the electronic detection system. Thus, the PL decay is obtained by a convolution of the measured signal with the response function of the TCPC system.

In the following all experimentally obtained time-resolved PL curves are the as-measured signals. The presented decay times have been extracted from fitting of the experimental data by a convolution procedure.

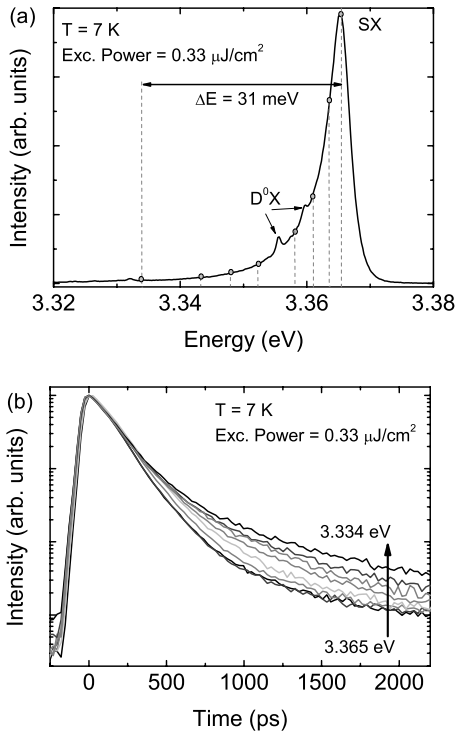

FIG. 2. (a) Spectrally resolved near-band-edge PL measured at low excitation intensity and low temperature. The dotted lines mark the spectral position at which transients (b) are measured.

III. EXPERIMENTAL RESULTS

In this section we present the investigations of the dynamics of the surface-related PL as a function of spectral position, temperature, and excitation intensity.

A. Dependence on the spectral position

In Fig. 2(a) the time integrated near-band-edge photoluminescence (PL) of the ZnO nanowire/nanowall system is shown at low temperature and low excitation fluence. The spectrum is strongly dominated by a broad asymmetric band peaked at ≈3.365 eV lying ≈9 meV below the free-exciton emission. Due to its spectral position and its excitation intensity dependence that will be presented in the following, this peak is assigned to the recombination of surface excitons (SX). This assignment is in agreement with the findings in Ref. 20–23. The shape of the SX band is similar to the one observed in Ref. 22. However, it is much more pronounced here and therefore can be clearly observed even on a linear scale. In addition to the dominant SX emission tiny contributions from the recombination of donor-bound excitons (D^0X) can be observed at the spectral positions of 3.356 and 3.360 eV. Contrary to the sample used in Ref. 20, where the PL is dominated by the D^0X lines the possibility is opened to investigate the SX band in detail without interfering with emission lines of other origin. The dominance of the SX peak is most probably due to the small diameters of the wires

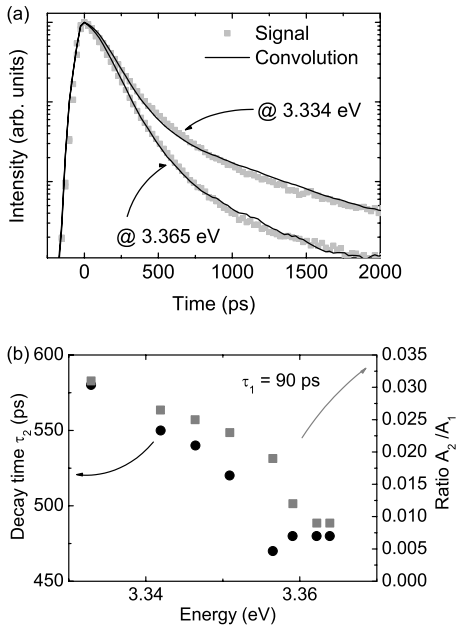

FIG. 3. (a) Grey curves: Transients measured at the spectral position of the SX peak maximum and 31 meV below. Black lines: Results of the convolution of the TCPC response function with the assumed biexponential decay. (b) Obtained decay times and ratio A_2/A_1 [Eq. (1)] vs spectral position.

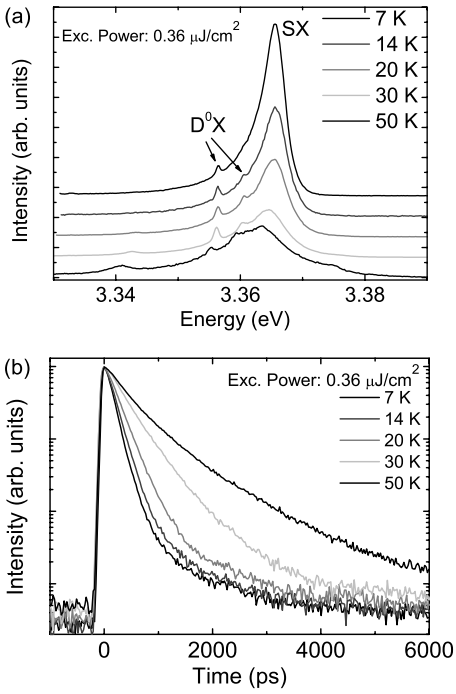

FIG. 4. (a) PL spectra taken at different temperatures. All spectra are normalized to the D^0X peak intensity and shifted in intensity. (b) Transients taken at different temperatures at the spectral position of the SX peak.

of $d=40$ to 130 nm resulting in an overwhelming contribution of the near-surface effects.

To get more information about the origin of this asymmetric band, transients on the maximum and at different spectral positions on the low-energy tail of the peak are measured. The spectral positions are marked by grey dots and dashed lines in Fig. 2(a), where the lowest detection position lies 31 meV below the SX peak. The transients are normalized and plotted in Fig. 2(b). The detected rise time of the signal is determined by the time resolution of the TCPC system. As mentioned above, the signal is a convolution of the response function of the detection system with the real PL decay. Thus, the characteristic decay data have to be derived by application of a convolution procedure. The temporal evolution then points to a biexponential PL decay which depends on the spectral position and can be described by

$$I(t) = \frac{1}{\tau_R - \tau_D}[e^{(-t/\tau_R)} - A_1 e^{(-t/\tau_1)} - A_2 e^{(-t/\tau_2)}] \qquad (1)$$

with $1/\tau_D = 1/\tau_1 + 1/\tau_2$. τ_R is the rise time, τ_1 and τ_2 are the decay times for a fast and a slow decay component, respectively. The factors A_1 and A_2 represent the fractions of the fast and the slow decay component, respectively. Due to the fact that different relaxation and recombination channels contribute to the measured signal the obtained decay times can not be directly assigned to life times of certain energy levels.

In general, the strongly pronounced SX emission indicates negligible nonradiative recombination. In Fig. 3(a) the measured transients taken at the peak maximum (3.365 eV) and 31 meV below this position (at 3.334 eV) are plotted (grey curves). The thin black lines in the same graph are the corresponding results of the convolution of the response function of the detection system with the biexponential decay given in Eq. (1) describing the evolution of the measured signal over three orders of magnitude. Within the experimental uncertainty a rise time of $\tau_R=20$ ps is obtained. The decay time τ_1 for the fast decay component obtained from the measured transients [Fig. 2(b)] amounts to about 90 ps and remains constant, independent of the detection energy. In contrast to this, the long decay time τ_2 of the slow component increases from 480 ps at the SX peak maximum to 580 ps at the detection energy of 3.334 eV [Fig. 3(b)]. Along with the increase of the decay time τ_2 the ratio A_2/A_1 increases which means that the fraction of the slow decay component increases.

Altogether, the asymmetric SX emission band consists of a whole distribution of SX states. The detected biexponential PL decay changes with the spectral position pointing to a dependence of the slow decay time τ_2 on a kind of localization of the excitons.

B. Temperature dependence

In Fig. 4(a) the PL spectra taken at low excitation power and different temperatures are plotted. All spectra are normalized to the D^0X peak intensity at 3.356 eV and offset in intensity for better visibility. At a temperature of 7 K the PL is dominated by the SX peak. With increasing temperature the SX-peak intensity decreases much faster compared to the D^0X peaks and has almost vanished at 50 K where the underlying D^0X emission peaks remain visible. At 50 K, an

TABLE I. Decay times (τ_1, τ_2) and ratio of both contributions (A_2/A_1) obtained by a convolution procedure from the transients shown in Fig. 4(b).

T [K]	τ_1 [ps]	τ_2 [ps]	A_2/A_1
7	90	500	0.0072
14	110	510	0.012
20	150	510	0.028
30	110	510	0.31
50	100	550	0.9

emission peak emerges at ≈3.375 eV which is assigned to the recombination of free excitons (FX). The observed rapid SX quenching points to a low activation energy which can be estimated roughly to 9 meV corresponding to its peak distance from the FX peak.

The corresponding transients taken at the spectral position of the SX peak at different temperatures are normalized and shown in Fig. 4(b). As described in Sec. III A, the decay times τ_1 and τ_2 as well as the ratio of the factors A_2 and A_1 are again obtained by the convolution procedure. The values are listed in Table I. Within the uncertainty both decay times remain constant with increasing temperature. However, the ratio A_2/A_1 increases by two orders of magnitude pointing to a thermal activation of the fast decay process (Fig. 4). Thus, the transients at elevated temperatures are dominated by the slow decay process.

Summarizing, the temperature dependence points to a thermal activation involved in the recombination and relaxation processes. The decrease of the PL intensity with increasing temperature suggests an activation of excitons trapped in SX states into free-exciton states (FX).

C. Intensity dependence

It is expected that the total number of near-surface states is lower than the total number of volume states. This means that the surface state transitions should saturate at a lower excitation intensity than those of the volume states. In Fig. 5(a) the PL spectra measured at low temperature and different excitation fluences are plotted. All spectra are normalized to the SX peak intensity and offset in intensity. At low excitation fluences the PL is strongly dominated by the SX emission. With increasing excitation fluence the D^0X peaks increase in intensity relative to the SX peak and finally dominate the spectrum. With increasing fluence no spectral shift is oberserved. In Fig. 5(b) the peak intensities at the spectral positions of the most intense D^0X and the SX peak are plotted versus the excitation fluence. Due to the spectral overlap of the D^0X and SX emissions the corresponding peak intensities are determined by this superposition. At elevated intensities the intensity increase of the D^0X line relative to the SX band [Fig. 5(a)] cannot be neglected and has to be taken into account. Thus, the SX peak intensities given in Fig. 5(b) are obtained by fitting the measured spectra with a superposition of two lorentzian curves. At low excitation fluences (<10 μJ/cm^2) the D^0X contribution is very small and

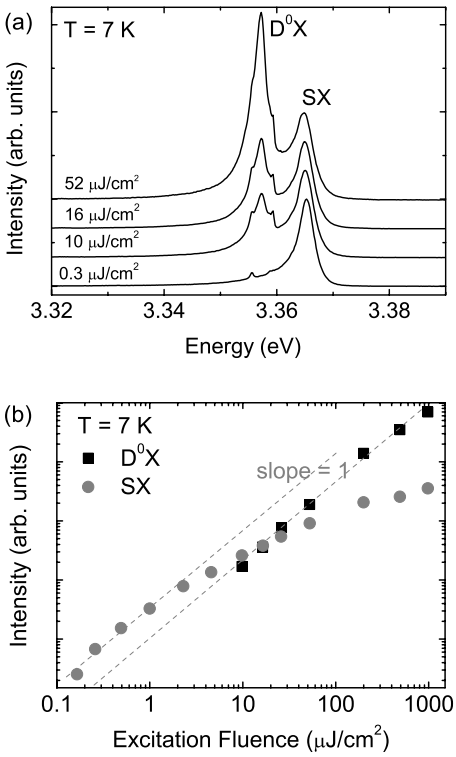

FIG. 5. (a) PL spectra taken at different excitation fluences. All spectra are normalized to the SX peak intensity and shifted in intensity. (b) Peak intensities at the spectral position of the most intense D^0X line and the SX peak as a function of excitation fluence.

thus prevents a clear analysis of its peak intensity. However, for elevated excitation fluences a linear increase of the intensity over three orders of magnitude is observed for the donor-bound exciton related emission. For the fluences applied here, saturation of D^0X emission is not yet reached. In contrast to this, for the SX peak an almost linear increase is observed at very low excitation intensities only. Above ≈1 μJ/cm^2 a clear saturation behavior is detected. This intensity dependence strongly deviating from that of D^0X supports the assignment of the SX peak to surface-related emission.

To analyze the SX dynamics as a function of excitation intensity, transients have been measured at the spectral position of the SX peak for different excitation fluences. With increasing excitation intensity the originally biexponential transient changes to an almost but not perfectly monoexponential shape [Fig. 6(a)]. In Fig. 6(b) the decay times as well as the ratio A_2/A_1 are shown as a function of excitation fluence. When increasing the excitation fluence over up to five orders of magnitude the fast decay time τ_1 increases from ≈110 ps up to ≈210 ps, whereas the slow decay time τ_2 remains constant at ≈500 ps. Along with the increase of τ_1 the ratio A_2/A_1 decreases by a factor of three and thus changes in favor of the fast decay. In contrast to this, at the spectral position of the D^0X peak a monoexponential decay with a time constant of τ=95 ps is observed which is independent of the excitation fluence as expected for donor-bound excitons.[29]

For the interpretation of the observed data we have to take into account the fact that the spectral overlap of both emis-

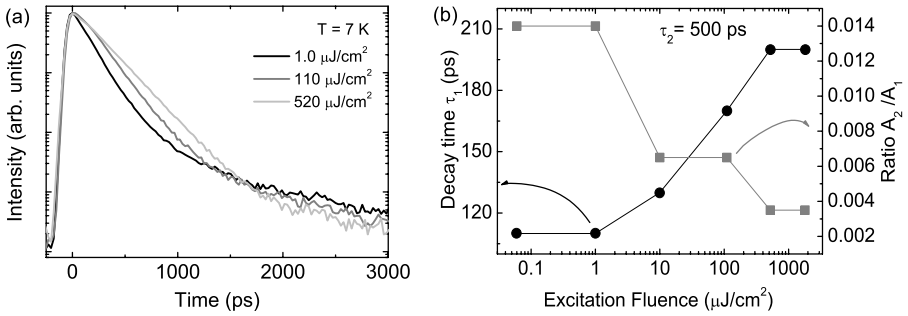

FIG. 6. (a) Transients measured at the SX peak position at different excitation fluences. (b) Obtained decay times τ_1 and τ_2 as well as the ratio of the contributions of both decay channels A_2/A_1 to the measured signal.

sion bands increases with increasing excitation fluence [see Fig. 5(a)]. The spectral overlap of an emission which decays monoexponentially (D^0X) with an emission showing a biexponential decay (SX) can be simulated just by a weighted sum of both decays. The ratio of both contributions to the resulting signal is determined by a weighing factor. The factor increases in favor of the monoexponential D^0X contribution with increasing excitation intensity. Doing this one result can be clearly observed. First, due to the fact that the D^0X decay time of ≈95 ps is somewhat smaller than the obtained fast decay time for the SX emission, the increasing spectral overlap would lead to a decreasing effective fast decay time with increasing excitation fluence. However, we have measured an increase of the fast decay time τ_1 which means that the observed behavior is a real SX band effect which is even partly suppressed by the spectral overlap with the D^0X emission. Second, the same simulation shows that the spectral overlap leads to a decrease of the fraction of the slow decay component what is not surprising. The increase of the fast decay time τ_1 with pump intensity seems to present only the density dependent feature of the SX emission and does correlate with the observed PL saturation behavior.

IV. SIMULATION AND DISCUSSION

Travnikov *et al.* have observed a likewise surface-related asymmetric emission in ZnO and CdS crystals.[22,25,26] It was assumed that in CdS crystals the line shape and especially the tail on the low-energy side is due to excitons localized at centers which have different distances to the sample surface. Such centers might be caused by impurities or structural defects. The near-band-edge PL of our ZnO-nanowire/nanowall system is dominated by a broad asymmetric peak. As is shown in Fig. 2(b) the transients taken at different energy positions along this peak can be described very well by a biexponentiel decay. To assign the observed decay times to relaxation and recombination processes of the excitons a simplified phenomenological rate-equation model is developed and discussed in the following to identify the most important processes.

An exciton trapped in the SX state 1 is either able to recombine with τ_{10} or to relax into centers at a lower lying energy (state 2) with τ_{12}. From there it can be thermally actived into the state 1 again at elevated temperatures (Fig. 7). The SX band is composed of the superposition of separated surface states with energies differing due to the varying local environment. This means that one has to integrate over the whole distribution of states 2. Just for reasons of simplicity, we summarize all states which are lower in energy than state 1 by one level only, since the basic characteristics of the whole surface states can be reproduced in very good agreement with this approximation, as we will show. This means that the level 1 represents the energy position at which the signal is detected. The level 2 summarizes the complete part of the band which is lower in energy than state 1. For interpretation of the observed dependence of the ratio A_1/A_2 on the spectral position the number of excitons is divided into two fractions as has been done by Neukirch *et al.* for the exciton relaxation in ultrathin single quantum wells.[27] In cases were the SX localization centers are very close to each other the excitons are able to recombine with a time constant τ_{10} or to relax by spatial migration into centers of lower energies with τ_{12}. Contrary, the excitons belonging to the second fraction are captured into locally isolated minima, most probably in regions of lower density of SX centers, and are thus unable to migrate but can recombine only with τ_{10}. For setting the rate equations, we call N_{1RR} and N_{1R} the number of states from which relaxation and recombination (1RR) or recombination only (1R) can take place, respectively. The division into these two fractions leads to the conclusion that the measured PL decay signal is a superposition of the observed biexponential decay and a monoexponential decay from isolated localized excitons. Due to the increase of the long decay time with decreasing detection energy we assign this decay to the pure recombination time τ_{i0} ($i=1,2$) of the excitons from the two SX states into the ground level 0 (Fig. 7). Based on the obtained energy dependence (Fig. 3) of $\tau_{i0}(E)$ it can be approximated by a linear interpolation between the decay times at 3.365 and 3.334 eV. In the

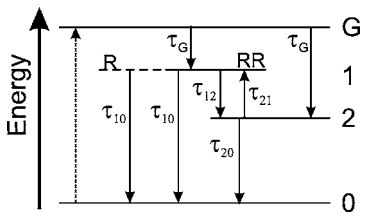

FIG. 7. Schematic energy diagram of used model discribing the excitation of excitons into state G and their relaxation or recombination pathways via the surface states 1 and 2. The level 1 has to be distinguished into weakly localized excitons that are able to relax and recombine (RR: solid line) and strongly localized excitons that are able to recombine only (R: dashed line).

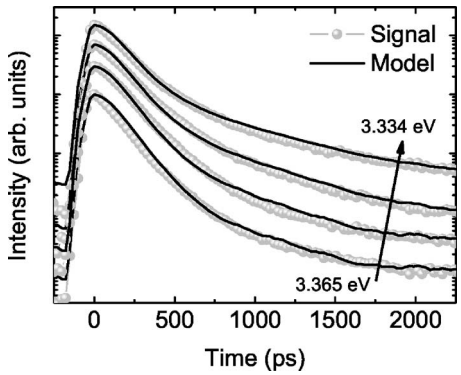

FIG. 8. Comparison of the measured transients (grey dots) and the results of the rate-equation model (solid lines) as function of detection energy. For the calculations a value of 0.003 in arb. units for the intensity and a temperature of 10 K were used.

temperature dependent measurement a quenching of the SX PL intensity was observed due to thermal activation of excitons trapped in SX states into free-exciton (FX) states. The excitons which are nonresonantly excited into the generation state G [occupation number $G(t)$] by a femtosecond pulse relax via the free exciton states into the SX and D^0X states. The latter will be ignored in the following. For simplicity, the complete pathway of the relaxation into the SX states is summarized by one step only with the relaxation time $\tau_G = 20$ ps, comparable to the observed rise time and much faster than the relaxation and recombination times. The detrapping or activation of excitons trapped to SX states into free-exciton states with increasing temperature will lead to an additional loss channel resulting in a decrease of the detected decay time. Due to the fact that the trapping rate of excitons into the SX states is given by $1/20\ \mathrm{ps}^{-1}$ and the activation energy is in the range of ≈ 9 meV corresponding to the energy separation between the FX- and SX-peak maxima, any expected variation of the decay time for temperatures up to 50 K remains within the experimental uncertainty and is thus negligible. With increasing temperature the trapped excitons can be activated from the lower level 2 into the nearest localization centers of the upper level 1RR by the rate $1/\tau_{21}$. To consider the SX saturation with increasing excitation intensity (Fig. 6) the limited total number of SX states is incorporated into the rate equations by a factor $M_i - N_i(t)$ where M_i $(i = 1\mathrm{R}, 1\mathrm{RR}, 2)$ gives the maximum occupation number of states 1R, 1RR, and 2, respectively. Taking all this into account we finally end up with the following system of rate equations:

$$\frac{dN_{1\mathrm{RR}}(t)}{dt} = -\frac{N_{1\mathrm{RR}}(t)}{\tau_{10}} - \frac{N_{1\mathrm{RR}}(t)}{\tau_{12}}[M_2 - N_2(t)] + \frac{N_2(t)}{\tau_{21}}[M_{1\mathrm{RR}} - N_{1\mathrm{RR}}(t)] + \frac{G(t)}{\tau_G}[M_{1\mathrm{RR}} - N_{1\mathrm{RR}}(t)], \tag{2}$$

$$\frac{dN_{1\mathrm{R}}(t)}{dt} = -\frac{N_{1\mathrm{R}}(t)}{\tau_{10}} + \frac{G(t)}{\tau_F}[M_{1\mathrm{R}} - N_{1\mathrm{R}}(t)], \tag{3}$$

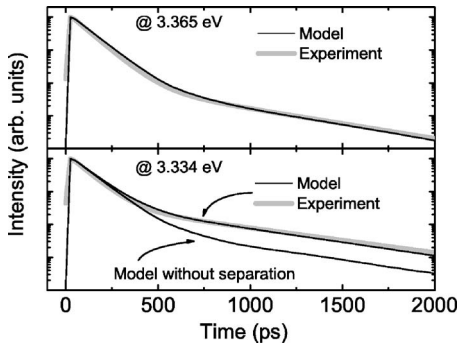

FIG. 9. (Upper graph) Comparison of transients obtained from the measured signal with the result of a rate-equation model at the spectral position of SX peak maximum. (Lower graph) Comparison of measured PL decay at 3.334 eV with results of the model without exciton separation and the expanded model. For the calculations a value of 0.003 in arb. units for the intensity and a temperature of 10 K were used.

$$\frac{dN_2(t)}{dt} = -\frac{N_2(t)}{\tau_{20}} + \frac{N_{1\mathrm{RR}}(t)}{\tau_{12}}[M_2 - N_2(t)] - \frac{N_2(t)}{\tau_{21}}[M_{1\mathrm{RR}} - N_{1\mathrm{RR}}(t)] + \frac{G(t)}{\tau_G}[M_2 - N_2(t)], \tag{4}$$

$$\frac{dG(t)}{dt} = -\frac{G(t)}{\tau_G}[M_{1\mathrm{R}} - N_{1\mathrm{R}}(t)] - \frac{G(t)}{\tau_G}[M_2 - N_2(t)] - \frac{G(t)}{\tau_G}[M_{1\mathrm{RR}} - N_{1\mathrm{RR}}(t)], \tag{5}$$

where the detected PL intensity is given by

$$I(t) \propto N_{1\mathrm{R}}(t) + N_{1\mathrm{RR}}(t). \tag{6}$$

For the calculation of the transients the generation time of excitons is suggested to be δ-like due to the fact that the length of the fs pulse is much shorter than the observed decay times. The number of generated excitons is thus defined

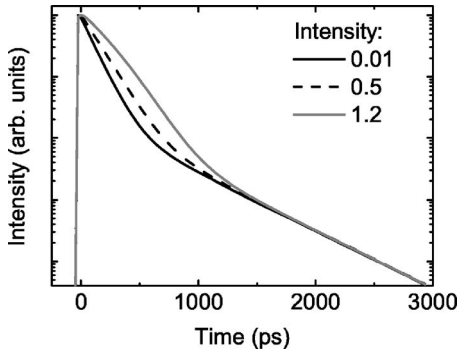

FIG. 10. Transients obtained from the rate-equation model as a function of excitation intensity at the spectral position of the SX-peak maximum. The intensities are given in arb. units representing the population of the generation state $G(t)$ at $t = 0$. The calculations have been performed for a temperature of 10 K.

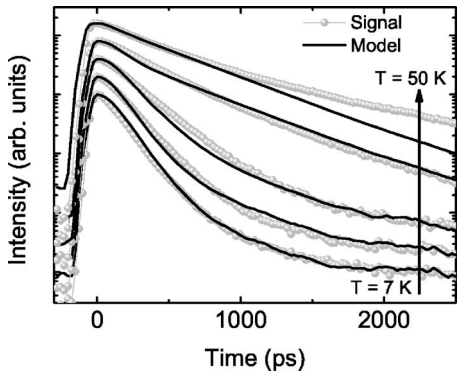

FIG. 11. Comparison of the measured transients (grey dots) at the spectral position of the SX-peak maximum and the results of the rate-equation model (solid lines) as function of temperature. For the fitting procedure a value of 0.003 in arb. units for the intensity and temperatures of 10, 11.6, 13.8, 30, and 52 K were used.

by the population $G(t)$ of the generation state at $t=0$.

In Figs. 8–11 the transients obtained from the rate-equation model are compared with the measured signals as functions of spectral position, excitation fluence, and temperature. For the comparison of the temperature and spectral position dependence the results of the calculations are convoluted with the response function of our detection system. In case of the excitation intensity dependence (Fig. 10) the calculated but nonconvoluted transients are plotted due to the fact that the spectral overlap between the D^0X line and the SX band leading to the change in the ratio A_2/A_1 is not taken into account in our model.

The total number of states M_{1RR} is set as 1. Consequently, the values for M_{1R}, and M_2 are set relative to $M_{1RR}=1$. For the comparison of the dependence on the spectral position the maximum number of states for strongly localized isolated excitons that are only able to recombine is chosen as $M_{1R}=0.0002$ at the spectral position of the SX peak maximum and is increased up to $M_{1R}=0.029$ for a detection energy of 3.334 eV to achieve best fitting results. The maximum number of N_2 states is set to $M_2=0.8$ for which the best fitting of the experimental results was achieved. The value of M_2 results from the assumption of two SX levels instead of a SX band and thus does not represent the real number of available states with an energy position lower than the detection energy. This values for the maximum number of states M_{1R}, M_{1RR}, and M_2 are used for all presented calculations. In Fig. 8 all curves are normalized and offset in intensity for a better overview. For the calculations of the transients as a function of detection energy a relaxation time τ_{12} of 90 ps was used. As intensity a value of 0.003 in arbitrary units was set within the rate-equation model representing the population of the generation state $G(t)$ at $t=0$. As can be clearly seen the dependence of PL decay on the spectral position in the as measured transients can be reproduced by our model very well. To analyze the influence of the exciton separation into strongly and weakly localized excitons, the as calculated transients without separation are compared to the nonconvoluted experimentally obtained PL transients. In the upper graph of Fig. 9 the transients at the spectral position of the SX peak maximum at ≈ 3.365 eV are compared. It can be clearly seen that both transients perfectly fit. For decreasing detection energy a deviation between the calculated and the experimental transients occurs and increases if the separation is not taken into account. This can be clearly seen in the lower graph of Fig. 9, where the obtained transients for the detection energy of 3.334 eV are plotted. The increasing deviation correlates to the increasing ratio A_2/A_1 (Fig. 3). It can be seen that at low temperatures the biexponential behavior is principally caused by the excitons that are strongly localized and thus are only able to recombine with the long decay time τ_{10}. If the separation at a suitable ratio M_{1R}/M_{1RR} is included, the experimental transients can be perfectly reproduced. These values for M_{1R}/M_{1RR} correspond to the ratio A_2/A_1 due to the fact that the maximum numbers of states 1R and 1RR determine the superposition of the fast and slow decays. The increase of the fraction of localized isolated excitons with decreasing detection energy may be explained as follows. The density of SX centers possesses its maximum at the sample surface and decreases with increasing distance to the surface resulting in a reduced tunneling probability by growing barrier width but most probably also in an overall enlargement of the potential barriers between the centers. Therefore, one expects an increasing fraction of strongly localized and thus isolated excitons. An increasing localization energy leads to a decreasing detection energy as well as to an increasing decay time as was observed in the experiment (Fig. 3). This is, by the way, analogous to the donor-bound exciton decay time, which also increases for growing binding energies.[29] A further microscopic interpretation of the spectral shift and the energy dependence of the decay time may be given by a result obtained by Satpathy.[28] It was shown that the hydrogenlike ground state of an electron on a donor changes continuously from 1S in the volume to 2P at the sample surface. Thus, the binding energy decreases with decreasing distance of the SX center to the surface.

The transients obtained from the rate equations with increasing excitation intensity are shown in Fig. 10. For the calculated transients the same saturation behavior as observed in the experiment can be seen. With increasing excitation intensity the increasing number of occupied SX states at lower lying energies lead to a decreasing transition rate $1/\tau_{12}$ and thus to an increase of the short decay time which is given by $1/\tau_1=1/\tau_{10}+1/\tau_{12}$. However, the intensities used for calculation and in the experiment are not directly comparable due to the two-level simplification of the SX band.

The temperature dependence of the measured signals and the calculated transients are compared and plotted in Fig. 11. The transients are normalized and offset in intensity. With increasing temperature the slow decay contribution increases while its decay time as well as that of the fast decay component remains constant within the experimental uncertainty. For the best reproduction of the experimental data temperatures of 10, 11.6, 13.8, 30, and 52 K were used for the calculations and are in good agreement with the nominal temperatures. Just for a temperature of 50 K a deviation occurs. This can be explained by the fact that the SX band has almost vanished at 50 K, i.e., the remaining donor-bound exciton emissions as well as the increased and broadened free-exciton emission (Fig. 4) contribute more strongly to the detected PL and thus lead to the observed deviation above

1 ns. A detailed analysis of the rate-equation model shows that for low temperatures the slow decay time is determined by the decay time τ_{20} of the lower SX level 2. With increasing temperature the probability of excitons recombining at level 2 decreases due to the thermally induced detrapping process into the upper level 1. Thus, the contribution of τ_{20} decreases in favor of the exciton recombination from state 1. This leads to an effective slow decay time determined by the pure recombination times τ_{10} and τ_{20} converging to τ_{10} with increasing temperature. Due to the small difference of $\approx$25 ps between $\tau_{10}(E)$ and $\tau_{20}(E)$ compared to their values which are in the range of about 500 ps a change in the effective and detected slow decay time cannot be resolved in the used experimental setup. Furthermore, it was found, not surprisingly, that the relaxation and activation processes between the levels 1 and 2 are correlated by

$$\tau_{21} = \tau_{12} \exp\left(\frac{\Delta E}{k_B T}\right) \tag{7}$$

with an activation energy of $\Delta E \approx 4.9$ meV. Due to the simplification of the whole SX band by two levels, the value of 4.9 meV must be interpreted as a mean energy which is needed for a detrapping into the SX states at higher energies.

V. CONCLUSION

In summary, we have analyzed the photoluminescence dynamics of surface-excitonic near-band-edge emission in a ZnO-nanowire system as a function of the spectral position, temperature, and excitation intensity. The observed findings were discussed by use of a simplified phenomenological rate-equation model describing the observed transients quite well by a biexponential decay. The measurements have clearly shown that an asymmetric surface-excitonic emission band is caused by a broad energy distribution of near-surface states. A detailed comparison between the experimental data and the rate-equation model has shown that the decay at low temperatures and low excitation intensity can be explained by excitons separated at each energy into a fraction of strongly localized and another fraction of weakly localized excitons. Thus, the observed trend towards longer decay characteristics for decreasing detection energy may be explained by the increase of the density of strongly localized excitons with increasing distance to the wire surface. The excitation intensity dependence has clearly shown that the limited number of near-surface states leads to a saturation with increasing excitation intensity resulting in an increase of the short decay component. The analysis of the temperature dependent measurements has revealed that originally trapped excitons are activated into near-surface states at higher energies with increasing temperature leading to an increasing fraction of the long decay time component. The presented results may stimulate further investigations and a careful determination of the microscopic origin of the surface-excitonic emission to either suppress it or to even make use of it in the design and operation of a future ZnO-based device.

ACKNOWLEDGMENTS

The authors thank the BMBF and European Union for their financial support through the projects NanoQuit and NANDOS, respectively.

*Electronic address: lars.wischmeier@ifp.uni-bremen.de
†Present address: Division of Engineering and Applied Sciences, Harvard University, Cambridge, MA 02138, USA.

[1] P. Yang, H. Yan, S. Mao, R. Russo, J. Johnston, R. Saykally, N. Morris, J. Pham, R. He, and H.-J. Choi, Adv. Funct. Mater. **12**, 323 (2002).
[2] Ü. Özgür, Y. I. Alivov, C. Liu, A. Teke, M. A. Reshchikov, S. Doğan, V. Avrutin, S.-J. Cho, and H. Morkoç, J. Appl. Phys. **98**, 041301 (2005).
[3] D. J. Sirbuly, M. Law, H. Yan, and P. Yang, J. Phys. Chem. B **109**, 15190 (2005).
[4] J. C. Johnson, H. Yan, R. D. Schaller, L. H. Haber, R. J. Saykally, and P. Yang, J. Phys. Chem. B **105**, 11387 (2001).
[5] M. H. Huang, S. Mao, H. Feick, H. Yan, Y. Wu, E. Weber, R. Russo, and P. Yang, Science **292**, 1897 (2001).
[6] G. C. Yi, C. Wang, and W. I. Park, Semicond. Sci. Technol. **20**, S22 (2005).
[7] X. Duan, Y. Huang, R. Agarwal, and C. M. Lieber, Nature (London) **421**, 241 (2003).
[8] J. C. Johnson, H.-J. Choi, K. P. Knutsen, R. D. Schaller, P. Yang, and R. J. Saykally, Nat. Mater. **1**, 106 (2002).
[9] Z. L. Wang, Mater. Today **6**(6), 26 (2004).
[10] L. Samuelson, Mater. Today **6**(10), 22 (2003).
[11] H. J. Fan, W. Lee, R. Scholz, A. Dadgar, A. Krost, K. Nielsch, and M. Zacharias, Nanotechnology **16**, 913 (2005).
[12] H. J. Fan, P. Werner, and M. Zacharias, Small **2**(6), 700 (2006).
[13] C. Klingshirn, R. Hauschild, H. Priller, M. Decker, J. Keller, and H. Kalt, Superlattices Microstruct. **38**, 209 (2005).
[14] C. Klingshirn, H. Priller, M. Decker, J. Brückner, H. Kalt, R. Hauschild, J. Zeller, A. Waag, A. Bakin, H. Wehmann, K. Thonke, R. Sauer, R. Kling, F. Reuss, and Ch. Kirchner, Adv. Solid State Phys. **45**, 261 (2005).
[15] A. Tsukazaki, A. Ohtomo, T. Onuma, M. Ohtani, T. Makino, M. Sumiya, K. Ohtani, S. F. Chichibu, S. Fuke, Y. Segawa, H. Ohno, H. Koinuma, and M. Kawasaki, Nat. Mater. **4**, 42 (2005).
[16] J. Xiang, W. Lu, Y. Hu, Y. Wu, H. Yan, and C. M. Lieber, Nature (London) **441**, 489 (2006).
[17] B. S. Kang, Y. W. Heo, L. C. Tien, D. P. Norton, F. Ren, B. P. Gila, and S. J. Pearton, Appl. Phys. A: Mater. Sci. Process. **80**, 1029 (2005).
[18] C. Thelander, T. Mårtensson, M. T. Björk, B. J. Ohlsson, M. W. Larsson, L. R. Wallenberg, and L. Samuelson, Appl. Phys. Lett. **83**, 2052 (2003).
[19] C. Lévy-Clément, R. Tena-Zaera, M. A. Ryan, A. Katty, and G. Hodes, Adv. Mater. (Weinheim, Ger.) **17**, 1512 (2005).
[20] L. Wischmeier, T. Voss, S. Börner, and W. Schade, Appl. Phys. A:

Mater. Sci. Process. **84**, 111 (2006).
[21] J. Grabowska, A. Meaney, K. K. Nanda, J.-P. Mosnier, M. O. Henry, J.-R. Duclere, and E. McGlynn, Phys. Rev. B **71**, 115439 (2005).
[22] V. V. Travnikov, A. Freiberg, and S. F. Savikhin, J. Lumin. **47**, 107 (1990).
[23] S. Savikhin, A. Freiberg, and V. V. Travnikov, JETP Lett. **50**, 122 (1989).
[24] A. C. Mofor, A. S. Bakin, A. Elshaer, D. Fuhrmann, F. Bertram, A. Hangleiter, J. Christen, and A. Waag, Prog. Solid State Chem. **3**, 1046 (2006).
[25] V. V. Travnikov, J. Cryst. Growth **101**, 579 (1990).
[26] V. V. Travnikov, Sov. Phys. Solid State **31**, 817 (1989).
[27] U. Neukirch, D. Weckendrup, W. Faschinger, P. Juza, and H. Sitter, J. Cryst. Growth **138**, 849 (1994).
[28] S. Satpathy, Phys. Rev. B **28**, 4585 (1983).
[29] J. Gutowski and A. Hoffmann, Adv. Mater. Opt. Electron. **3**, 15 (1994).